Particle Accelerators, 1989, Vol. 25, pp. 43–56
Reprints available directly from the publisher
Photocopying permitted by license only

Printed in the United States of America

SIMULATION STUDIES OF PARTICLE ACCELERATION POWERED BY MODULATED INTENSE RELATIVISTIC ELECTRON BEAMS†

J. KRALL
Science Applications Intl. Corporation, McLean, VA

V. SERLIN, M. FRIEDMAN and Y. Y. LAU
Plasma Physics Division, Naval Research Laboratory, Washington, DC 20375-5000

(Received March 8, 1989)

A time-dependent, fully electromagnetic particle code is used to simulate transfer of energy from an annular modulated intense relativistic electron beam to a low-current electron beam via a disk-loaded structure. It is shown that an intense beam may be used to drive such an accelerator at a high transformer ratio ($R \simeq 10$) to obtain accelerating gradients in the ~100 MV/m range, with power in excess of 1 GW transferred from the primary to the secondary beam.

1. INTRODUCTION

Future progress in accelerators and their applications may depend critically on the development of physical mechanisms capable of generating high voltage gradients. It has been shown that a high electric field can be established in rf structures by modulated intense relativistic electron beams (MIREBs) of power greater than 10^9 W and that such a beam may be used as an rf source to power an accelerator, obtaining voltage gradients as high as 100 MeV/m or greater.[1,2] Such an accelerator, in which a low-energy, high-current beam interacts via a metallic structure with a low-current beam to obtain very high energies, has been suggested by a number of authors, including Voss and Weiland,[3] and is outlined in Ref. 2. Wakefield acceleration has recently been observed in experiments carried out by Figueroa *et al.*[4]

Theoretical discussions of accelerators powered by MIREBs[2,5,6] have suggested unusual properties that may be present in such devices. First, the demonstrated conversion of the high dc power of an intense relativistic electron beam (IREB) to high rf power in the MIREB by the use of tuned radial cavities implies that the MIREB may be coupled to an rf structure so as to drain significant power (>1 GW) from the beam at high efficiency. Second, geometrical effects may allow for sizeable variations in efficiency, field gradient, and coupling between the

† Work supported by the Department of Energy under Contract No. DE-AI05-86-ER13585.

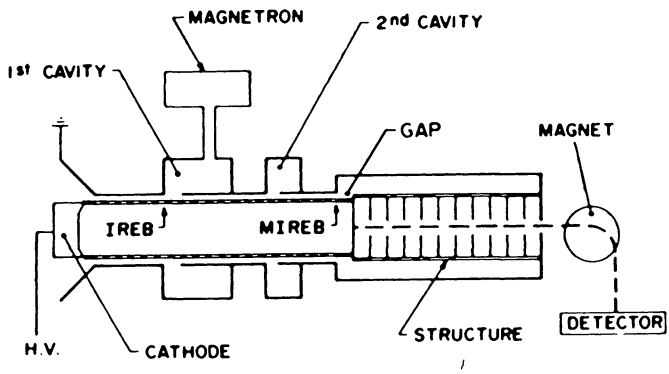

FIGURE 1 MIREB-driven accelerator schematic.

high-power MIREB and the rf structure with small changes in the experimental parameters.

In this paper we study these issues via an axisymmetric particle simulation using the CONDOR[7] code, which has been previously and successfully applied to the physics of such intense beams.[8] The accelerator configuration to be studied is similar to that outlined in Ref. 2 and is depicted in Fig. 1.

1. An annular IREB generator injects a beam of radius $r_b \simeq 6.3\,\text{cm}$, current $I_0 = 16\,\text{kA}$, energy $E_{inj} = 500\,\text{keV}$ and duration $T = 150\,\text{ns}$ into a drift tube of radius $r_w = 6.8\,\text{cm}$. The IREB is guided by an axial field $B_0 = 10\,\text{kG}$.

2. The IREB is fully modulated at $f \simeq 1.3\,\text{GHz}$ by a pair of tuned radial cavities, the first of which is externally driven by a low-level rf source (magnetron). The modulation region is immersed in the axial magnetic field.

3. The MIREB is guided into a cylindrical cavity of radius 9.6 cm. The cavity is loaded with thin disks of radius 9.0 cm and separation 1.88 cm. The MIREB, which has a frequency of modulation corresponding to the desired mode of the rf structure, is terminated at the first disk. A resonant interaction occurs at the gap defined by the end of the drift tube and the first disk of the rf structure, transferring energy from the beam to the rf structure.

4. An emitter, located on-axis on the surface of the first disk, emits electrons when the fields within the structure reach a sufficiently high value. This secondary beam is then accelerated by the rf fields, guided by the axial magnetic field.

The modulation stage of this device has been studied in some detail for a 1.9 cm radius annular beam in a 2.4 cm radius drift tube[6,8,9] and has been successfully repeated at $I_0 = 16\,\text{kA}$ and $r_b = 6.3\,\text{cm}$ in a drift tube of radius 6.8 cm.[10]

In this paper, we will investigate the coupling between the modulated beam and the rf structure and the subsequent acceleration of the secondary beam and shall proceed as follows. In Section 2, we give theoretical background on the expected field gradients in the rf structure, define a transformer ratio for this acceleration scheme, and present numerical results from the SUPERFISH[11] code on the modes of the rf structure. In Section 3, which contains the main results of this

paper, we will simulate particle acceleration and will see that power in excess of 1 GW may be transferred between the primary and secondary beams. Here we will consider the effect of geometrical variations on the beam-rf structure coupling and on the transformer ratio. Section 4 will contain a detailed discussion of the numerical issues that affect the ability of these simulations to correctly predict experimental results. Section 5 concludes.

2. FIELDS IN THE RF STRUCTURE

The process of energy transfer between the primary and secondary beams in this accelerator resembles that of the wakefield schemes described in Refs. 3 and 4 in the use of fields excited by the primary beam in a disk-loaded structure. In these schemes, the two beams travel colinearly such that the transformer ratio is defined as $R = E_2/E_1$, where E_1 is the magnitude of the decelerating field experienced by the primary beam and E_2 is the accelerating gradient experienced by the secondary beam. In the present case, however, the interaction of the primary beam with the rf structure takes place only as the beam traverses the gap near the first disk of the rf structure, where the beam is terminated, while the secondary beam is accelerated along the entire length of the rf structure. The transformer ratio is then defined as

$$R = \frac{\langle E_{\text{axis}} \rangle L}{E_{\text{gap}} d}, \tag{1}$$

where d is the gap length, L is length of the rf structure, E_{gap} is the decelerating field in the gap (assumed to be spatially constant) and $\langle E_{\text{axis}} \rangle$ is the average field experienced by the accelerated secondary-beam particles.

This geometry has been modeled as an interaction between a sinusoidally varying current source and a transmission line consisting of a series of R–L–C circuit elements.[2] This model exhibited many features that have been found in the numerical simulations, but such a model has a limited predictive capability.

Some insight into this problem may be obtained by assuming that the disk structure will behave like a resonant cavity. One may solve for the normal modes of this cavity by neglecting the interaction region at the gap.[2] For the purposes of this discussion, however, we may consider the only fundamental mode of a disk-loaded cavity of length $L = n\lambda/2$, where λ is the wavelength of the rf and n is a positive integer. In this case, the z-component of the electric field of the fundamental mode varies sinusoidally along the axis and radially as

$$E_z(r)/E_z(r=0) = J_0(kr)/J_0(r=0), \tag{2}$$

where J_0 is a Bessel function and $k = 2\pi/\lambda$. In the analysis of Ref. 2, it was conjectured via a heuristic argument that the ratio of the field experienced at the gap by the primary beam ($r = r_b$) to the peak field on-axis ($r = 0$) would follow this radial variation. This suggests that the radial position of the primary beam in relation to the mode structure within the rf cavity is of some importance for the strength of the interaction, the efficiency, and the obtainable transformer ratio.

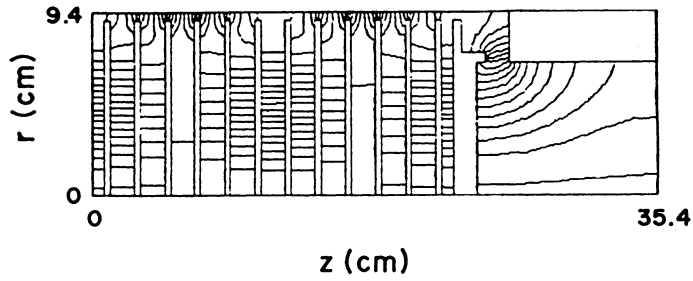

FIGURE 2 SUPERFISH result showing the electric field configuration of an rf structure cavity mode with frequency 1.33 GHz.

The normal modes for a given axisymmetric cavity may be calculated numerically by using the SUPERFISH[11] code. The SUPERFISH result for one such cavity is shown in Fig. 2. Here, a disk-loaded cavity of length $L \simeq \lambda$ is used and the gap region is included. Except for the metallic boundary condition imposed at the right-hand wall, this geometry closely resembles that of Fig. 1, where the right-hand boundary is an open drift tube for which the 1.33-GHz cavity mode is below cutoff. This result and a series of similar results, where the location of the right-hand wall was varied, show that the expected cavity mode is obtained.

3. NUMERICAL SIMULATIONS

The simulation geometry (Fig. 3) consists of a short drift-tube region with radius $r_w = 6.8\,\text{cm}$, a gap of length $d = 1.57\,\text{cm}$, and a disk-loaded structure of length $L = 22.2\,\text{cm} \simeq \lambda$. Here $\lambda = c/f$ and $f = 1.27\,\text{GHz}$ is the numerically determined frequency of the accelerating mode of the cavity.

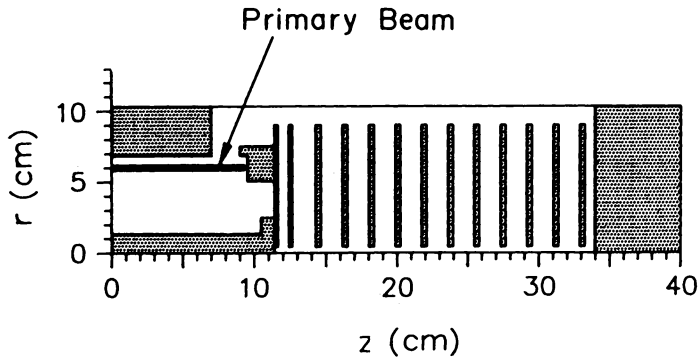

FIGURE 3. Simulation geometry showing the primary beam and the disk-loaded rf structure. The primary beam enters the drift tube region from the left, passes near the gap at $z \simeq 8\,\text{cm}$ and is terminated at $z \simeq 9\,\text{cm}$. The secondary beam is injected at $z \simeq 12\,\text{cm}$ and is accelerated along the axis.

The primary beam is injected from the left-hand wall with radius $r_b = 6.4$ cm, energy $E_{inj} = 2.0$ MeV and current $I_{inj}(kA) = g(t)\,[16 + 8\sin(2\pi ft)]$, where $g(t)$ is an envelope function that increases linearly from zero to unity during the time $0 < t < 15$ ns and remains constant thereafter. At a selected time, $t > 15$ ns, the secondary beam with $I_2 = 10$ Amperes and $E_2 = 0.1$ MeV is injected continuously from the center of the first disk and is accelerated along the axis by the rf fields. Each simulation continues until $t = 30$ ns.

Note that in order for the cavity-mode approximation of Section 2 to be of use, the parameters L, v_g and T must be such that $L/v_g \ll T$, where v_g is the group velocity of E-M radiation within the disk-loaded structure and T is the duration of the primary beam pulse. If this relation is not satisfied, the disk structure will behave not like a cavity, but like a traveling wave tube. In the numerical geometry of Fig. 3, we have arranged the separation between the outer disk edges and the cavity wall so that $v_g/c \simeq 1$. In this case the condition $L/v_g \ll T$ is easily satisfied within the 30-ns duration of the simulations.

Several differences between this configuration and that of a practical experi ment must be noted.

1. In a practical experiment the disk structure would be longer so as to obtain higher energies in the secondary beam. Another difficulty is that the high group velocity of the E-M waves in the simulation structure, along with its short length and small volume, will allow rf fields to build up so quickly that they would reflect the primary beam if the simulation continued long enough.

2. An actual device would have support rods to hold the disks in place.[2] These would also provide a path for the dc current of the primary beam. Because such supports cannot be modelled axisymmetrically and because we require a dc current path, we inserted a center conductor to serve this purpose. It will be seen in Section 4, below, that the presence of this center conductor does not significantly affect the results.

3. In the simulation geometry, the left-hand boundary is a metallic wall. In an actual device and in Fig. 1, this boundary is an open drift tube, for which the 1.27 GHz frequency of the rf field is below cutoff. The metal boundary of the simulations will have a similar effect of reflecting incident radiation at this frequency, but is clearly not the same.

4. The simulation structures are defined on a grid such that the effective skin depth of the material is one grid cell ($\Delta r = 0.2$ cm, $\Delta z = 0.3133$ cm), making the cavity extremely lossy, with Q of order 10. A typical Q value for a metallic structure is of the order 1000.

Figures 4 and 5 show the z-component of the electric field plotted vs. time in the gap and on-axis, respectively, for a simulation with parameters described above. The plot on-axis is taken at the spatial location of the peak electric field. We see that the fields increase continuously, reaching values of 56.3 MV/m at the gap and 94.2 MV/m on-axis before the simulation is halted. The plot of the gap electric field shows evidence of a weak lower-frequency mode, which may have been excited by the increase in dc current from $t = 0$ to $t = 15$ ns. The rf cavity mode, as expected, is a standing wave, varying in z sinusoidally and radially as a

Bessel function, $J_0(kr)$. This is seen in Figs. 6 and 7, which show E_z vs. z and E_z vs. r, respectively, at a fixed time.

For the simulation shown, the secondary beam was injected continuously for $t > 17$ ns with $I_2 = 10$ A and $E_2 = 0.1$ MeV, and was bunched and accelerated by the rf fields. This acceleration may be observed in Fig. 8, which plots particle positions in phase space, $\gamma\beta c$ vs. z, where β is the axial particle velocity normalized to c and $\gamma = (1 - \beta^2)^{-1/2}$. The particle positions, plotted at fixed time at intervals of 0.2 ns, show a maximum energy increase of 8.60 MeV over 22.2 cm to give an accelerating gradient of 39.2 MV/m. With this result and the observed 56.3 MV/m fields at the gap, we see that for this case a transformer ratio $R = 9.85$ is achieved.

Several interesting aspects of this simulation should be noted.

1. The build up of rf in the cavity is of a transient nature. Were the simulation not halted at $t = 30$ ns, the field amplitudes would increase beyond the observed 94.2 MV/m until limited by reflection of the primary beam. In an actual device, other limitations may include breakdown in the rf structure, losses due to the Q of the cavity, termination of the primary beam, or acceleration of a sufficiently high quantity of secondary beam current.

2. The conjectured relationship between the gap field, E_{gap}, and the peak axial field, E_{axis}, which was discussed in connection with Eq. (2) above, does not hold. Here, we have $E_{\text{axis}}/E_{\text{gap}} = 1.67$ and $J_0(0)/J_0(kr_b) = 2.51$. While the conjectured relationship does not hold in a precise way, it may still be useful as a qualitative guide. We still expect that an increase in $J_0(0)/J_0(kr_b)$, obtainable by increasing r_b, will result in an increased $E_{\text{axis}}/E_{\text{gap}}$. This has been investigated and is described below.

3. The electric field of 56.3 MV/m observed across the 1.57 cm gap indicates that the primary beam loses 0.883 MV as it traverses the gap. This energy loss is verified in the phase-space plots of Fig. 8, where the primary beam particles, at $0 < z < 10$ cm, are deflected in momentum space by the gap voltage. This indicates a power drain of 7.07 GW at 1.27 GHz and is sufficient power to accelerate secondary beam currents in the 500–A range over this short distance. With a longer accelerating structure, beams of lower currents may be accelerated to higher energies.

To test our conjecture that higher current may be accelerated to obtain high power in the secondary beam, we repeated the simulation of Figs. 4–8 with the secondary beam current increased to 200 A. We found $E_{\text{gap}} = 51.6$ MV/m and $E_{\text{axis}} = 91.3$ MV/m. Secondary beam particles, injected at 0.1 MeV, were accelerated to 8.02 MeV to give $\langle E_{\text{axis}} \rangle = 35.7$ MV/m so that $R = 9.78$. A comparison of these results with those of Figs. 4–8 indicates that the 200 A secondary beam does not significantly load the cavity. We also see that 1.58 GW of rf power has been transferred from the primary to the secondary beam.

While the supposed relationship between E_{gap} and E_{axis} discussed in connection with Eq. (2) has already been proven imprecise, there remains an intriguing possibility of obtaining very high transformer ratios as the primary beam radius approaches $r_b = j_{0,1}/k$, where $J_0(j_{0,1}) = 0$. We investigated this by repeating the

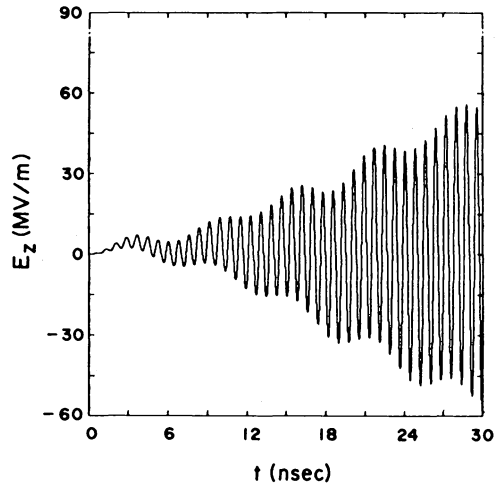

FIGURE 4. E_z plotted versus time at the gap for the $r_b = 6.4$ cm case.

simulation of Figs. 4–8 with $r_b = 8.0$ cm. This required an increase in the drift tube radius to $r_w = 8.4$ cm, a change in geometry which shifted the resonance slightly to 1.34 GHz. At this frequency, $j_{0,1}/k = 8.57$ cm. The results of the simulation are shown in Figs. 9–12. We found field gradients of $E_{\text{gap}} =$ 13.5 MV/m and $E_{\text{axis}} = 34.4$ MV/m. Particle plots (not shown) indicated that the secondary beam particles, injected at 0.1 MeV, were accelerated to 3.27 MeV to give $\langle E_{\text{axis}} \rangle = 14.3$ MV/m so that R has been increased to 15.0. Figures 9–12

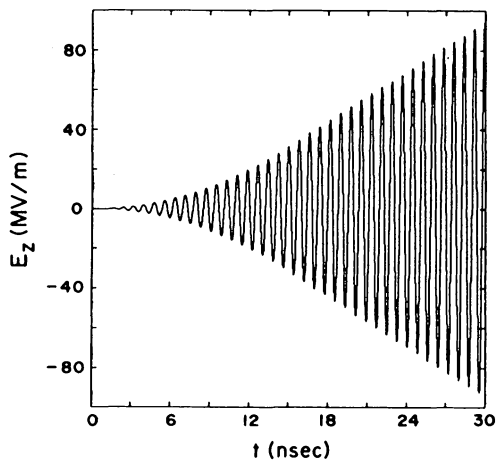

FIGURE 5. E_z versus time on-axis at $z = 20.6$ cm, near the point of peak axial field.

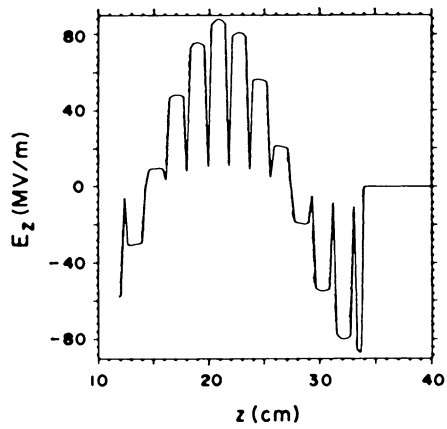

FIGURE 6. E_z versus z plotted on-axis at $t = 28.4$ ns.

contain the following results:

1. With $r_b = 8.0$, we have $E_{axis}/E_{gap} = 2.55$, an increase from the value of 1.67 that was obtained at $r_b = 6.4$ cm, but not nearly as large as $J_0(0)/J_0(kr_b) = 11.9$. Note that the transformer ratio was similarly increased, from 9.85 to 15.0. As stated above, we have only a qualitative ability to predict results as r_b is changed.

2. Figures 9 and 10 show that the build-up of rf fields in the cavity is of a transient nature, as before, but much lower amplitudes are reached at $t = 30$ ns than in the $r_b = 6.4$ cm case. This indicates that as the E_{axis}/E_{gap} ratio is increased, the interaction between the primary beam and the rf structure is weakened. This occurs because, at a higher transformer ratio, the same accelerating field in the rf structure gives a lower decelerating field at the gap and less energy is drained from the primary beam per cycle. After a long enough time, the fields in such a system will build up to the point where the full energy is drained from the primary beam and an extremely high axial field is obtained. The low frequency

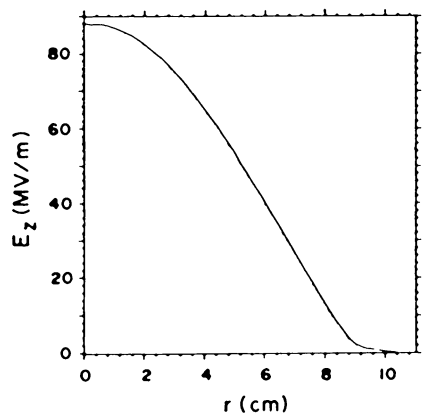

FIGURE 7. E_z versus r plotted near the point of peak axial field, $z = 20.6$ cm, at $t = 28.4$ ns.

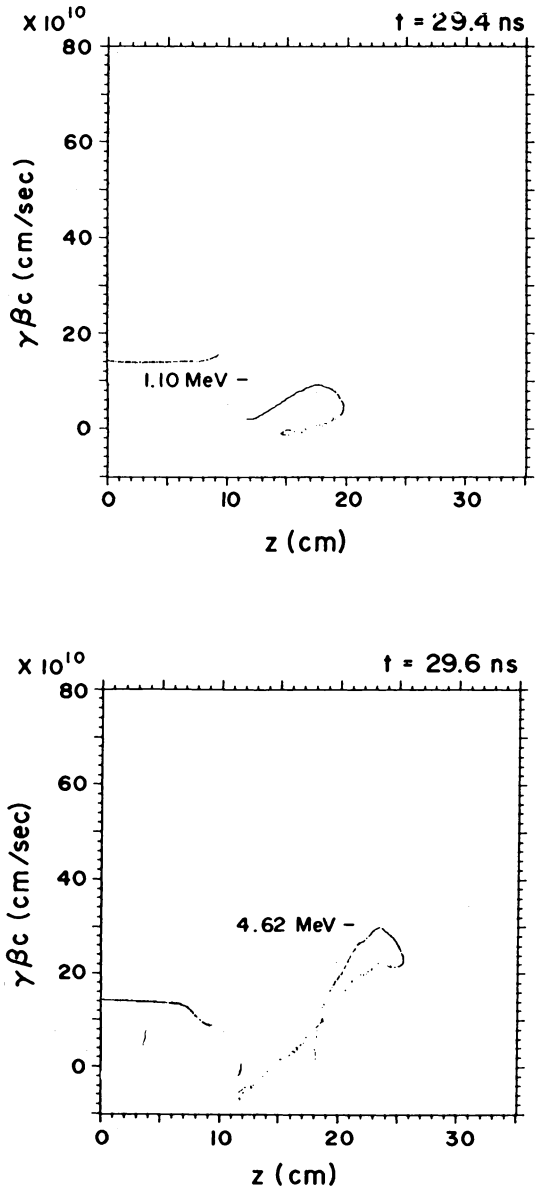

FIGURE 8. Particle positions in phase-space, $\gamma\beta_z c$ versus z, at intervals of 0.2 ns. The primary beam is on the left, $0 < z < 10$ cm. The peak energy of the accelerating secondary beam particles is noted on each plot.

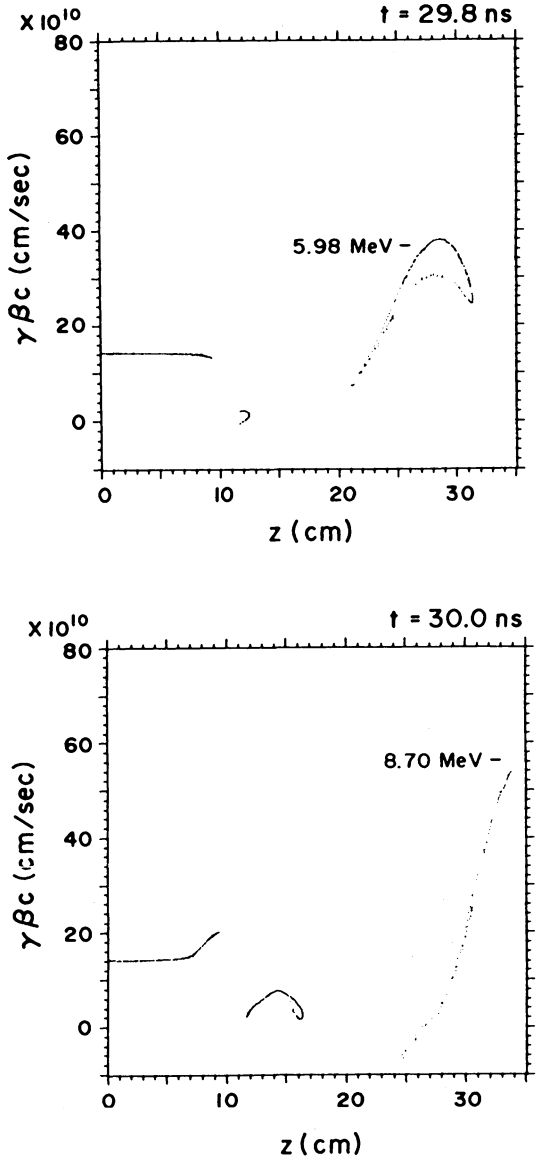

FIGURE 8. (*contd.*)

excitation of the cavity, apparent in Figs. 4 and 9, is unchanged, making it more prominent in the latter case where the rf fields are weaker.

3. The peak electric field on-axis, plotted in Fig. 10, appears to be saturating as the simulation is terminated. It is not clear whether this is a result of the low Q of the numerical structure or if we are driving the cavity slightly off-resonance. We can also see, from Figs. 11 and 12, that the mode structure is unchanged from the previous cases.

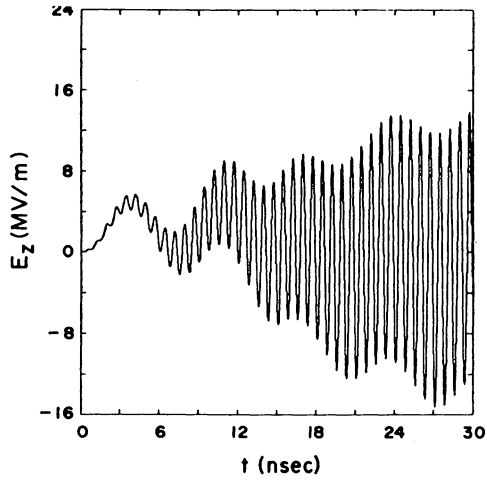

FIGURE 9. E_z versus t at the gap for the $r_b = 8.0$ cm case.

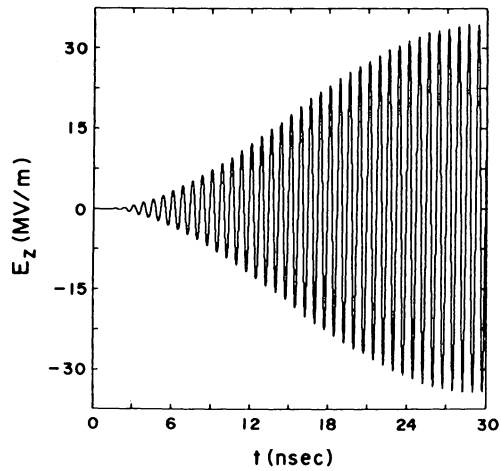

FIGURE 10. E_z versus t on-axis at $z = 22.6$ cm, near the point of peak axial field.

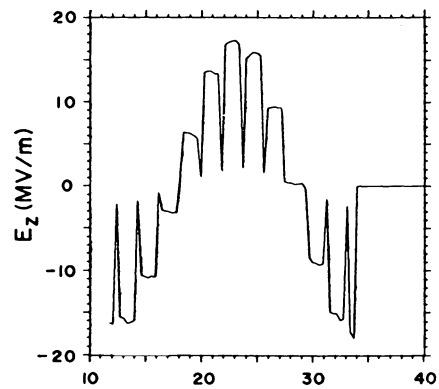

FIGURE 11. E_z versus z on-axis at $t = 30.0$ ns.

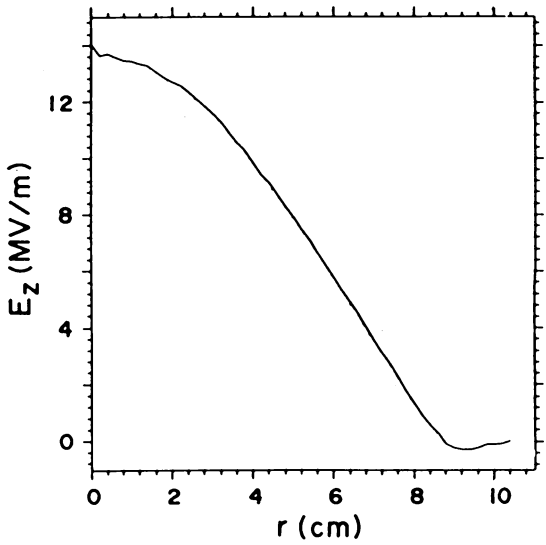

FIGURE 12. E_z versus r near the point of peak axial field, $z = 20.6$ cm, at $t = 30$ ns.

Finally, we must note that at $r_w = 8.4$ cm, $f = 1.34$ GHz is very close to the cutoff frequency f_c, which is given by $j_{0,1}c/2\pi r_w = 1.37$ GHz. In a practical device, it may not be possible to increase r_b and r_w to such large values at this frequency.

4. NUMERICAL EFFECTS

To understand the applicability of the simulation results to an actual device, it is necessary to examine the differences between such a device and the numerical model. Many of these have already been addressed. One which was not addressed is the addition of a center conductor to the drift-tube region of the simulation geometry, which provides a path for the dc component of the primary beam current. The significance of this addition may be examined by considering equivalent circuit elements for the rf structure (a capacitive load) and the center conductor (an inductive load). These elements are connected in parallel and are driven by an oscillatory current source. The inductance of a coaxial line varies as $L \propto \log(r_w/r_c)$, where r_c is the radius of the center conductor. The equivalent circuit model suggests that an increase in r_c will lower the inductive load relative to the capacitive load, lowering the voltage across the capacitance. This was verified by increasing the radius of the center conductor to $r_c = 5.0$ cm in the $r_b = 6.4$ cm case. This had the effect of lowering the field amplitudes in the gap and on-axis by a factor of 1.7, but left the transformer ratio unchanged. Conversely, the circuit model suggests that, for sufficiently small values of r_c, the inductance will be so high as to behave like an open circuit. In this ideal case, the entire load lies across the capacitance.

To discover whether or not the radius of the center conductor is sufficiently small, we repeated the $r_b = 6.4$ cm simulation with the dc component of the primary beam current removed, so that $I_{inj}(kA) = g(t)8 \sin(2\pi ft)$, where $g(t)$ is an envelope function as before. This was accomplished by superimposing an appropriately modulated electron beam with a dc positron beam, and allowed us to compare results with and without the presence of the center conductor. With the center conductor, we found $E_{gap} = 56.1$ MV/m, $E_{axis} = 92.6$ MV/m, and $\langle E_{axis} \rangle = 38.8$ MV/m, comparable to the results of Figs. 4–8. Without the center conductor, we found $E_{gap} = 60.0$ MV/m, $E_{axis} = 103.6$ MV/m, and $\langle E_{axis} \rangle = 41.5$ MV/m. This indicates that the presence of the center conductor reduces the fields by *5–10%*.

5. CONCLUSIONS

We have shown that high fields and transformer ratios can be supported by a MIREB-driven accelerator, demonstrating several interesting properties. The most crucial of these is that the MIREB is so strongly coupled to the disk-loaded rf structure that power in excess of 1 GW may be transferred from the primary to the secondary beam despite the low Q of the numerical structure.

We have found that the build up of the rf fields in the structure is transient by nature and, in the simulations, peak accelerating gradients were limited only by the brevity of the simulations. In an actual device, these fields will continue to increase in amplitude until limited by breakdown in the rf structure, reflection of the primary beam at the gap, or termination of the primary beam pulse.

We have also considered variations of the geometry to successfully obtain an increased transformer ratio, but at the cost of weakening the coupling between the primary beam and the rf structure. We have also found that the conjectured relationship between the decelerating field experienced by the primary beam at the gap and the peak accelerating gradient on-axis, which is discussed in connection with Eq. (2), provides only a qualitative guide to these geometric variations. As the original conjecture, contained in Ref. 2, is heuristic in nature and pertains to an idealized physical model, this is not a surprising result.

Finally, the differences between these simulations and a practical experimental configuration have been discussed in some detail, suggesting that similar power levels, fields, and transformer ratios may be obtainable experimentally.

REFERENCES

1. M. Friedman and V. Serlin, *Phys. Rev. Lett.* **55,** 2860 (1985).
2. M. Friedman and V. Serlin, *Appl. Phys. Lett.* **49,** 596 (1986).
3. G. Voss and T. Weiland, DESY Report M82-10 and DESY Report M82079 (1982).
4. H. Figueroa, W. Gai, R. Konecny, J. Norem, A. Ruggiero, P. Schoessow and J. Simpson, *Phys. Rev. Lett.* **60,** 2144 (1988).
5. Y. Y. Lau, *J. Appl. Phys.* **62,** 351 (1987).
6. M. Friedman, J. Krall, Y. Y. Lau and V. Serlin, *J. Appl. Phys.* **64,** 3353 (1988).

7. CONDOR is an extension of the MASK particle code, discussed in A. Palevsky and A. Drobot, in the *Proceedings* of the Ninth Conference on Numerical Simulation of Plasmas, July 1980 (Northwestern University, Evanston, IL) (unpublished).
8. J. Krall and Y. Y. Lau, *Appl. Phys. Lett.* **52,** 431 (1988).
9. Y. Y. Lau, J. Krall, M. Friedman and V. Serlin, *IEEE Trans. Plas. Sci.* **16-2,** 249 (1988).
10. M. Friedman, V. Serlin, Y. Y. Lau and J. Krall (to be published).
11. K. H. Halbach and R. F. Holsinger, Lawrence Beskeler Laboratory report LBL-5040 (1976).